

## Wake Flows in Coastal Oceans: An Experimental Study of Topographic Effects

M. J. O'Byrne<sup>1</sup>, R. W. Griffiths<sup>1</sup> and G. O. Hughes<sup>1</sup>

<sup>1</sup>Research School of Earth Sciences,  
 The Australian National University, Canberra, ACT, 0200, Australia

### Abstract

We consider the effects of coastal topography on the wake of an idealised headland model in a laboratory flume. Under a range of Reynolds numbers relevant to coastal oceans, we find that coherent eddies interact strongly with the headland shear layer and wake, affecting the width of the shear layer and the length of the wake. A preliminary investigation of turbulence statistics indicates that topography upstream of a headland can lead to a wider shear layer, a headland wake that extends further downstream, and enhanced horizontal diffusion out of the wake relative to the case with unperturbed oncoming flow.

### Introduction

Flow around coastal topography usually involves strong wakes with vigorous recirculation after separation from the coastline. These wake flows and their associated eddies trap suspended particles, bring nutrients up from deeper waters and influence the deposition of sediments. Characterising them is important to waste disposal, the positioning of sewer outlets, the location of fisheries and recreational pursuits.

Field studies and numerical work indicate that disturbances upstream of islands or headlands can trigger instabilities in the wake. Only certain topographical features appear to produce large-scale eddies despite typically strong currents [1, 4, 7].

Figure 1 shows the flow pattern past Bass Point, a coastal headland 100 km south of Sydney (adapted from [4]). When a long-shore current passes the headland, flow typically separates from the coastline. This separated flow has a very strong shear layer which injects strong vorticity into the lee of the headland. This can cause a large-scale eddy to form, as seen in figure 1. In some cases, a string of vortices may also be generated [6].

The most important dimensionless quantity for studying the transition to turbulence is the Reynolds number [2]:

$$Re = \frac{uL}{\nu}, \quad (1)$$

where  $u$  and  $L$  are characteristic velocity and length scales of the flow and  $\nu$  is the kinematic viscosity of the fluid.

In oceanic flows it is more meaningful to evaluate the horizontal Reynolds number,  $Re_x$ , using the horizontal eddy diffusivity  $\nu_x$ , a quantity characterising horizontal turbulent diffusion. The typical eddy diffusivity in coastal regions such as Bass Point is  $\nu_x \sim 1 \text{ m}^2 \text{ s}^{-1}$ , with length scale  $L \sim 10^3 \text{ m}$  and flow speed  $u \sim 1 \text{ ms}^{-1}$ , giving  $Re_x \sim 1000$  [6]. The range of Reynolds numbers used in the laboratory experiments discussed here, based on the headland length scale, straddles this regime of interest.

In this paper we investigate the effects of incident disturbances on instability in the wake of a semi-cylindrical headland and seek an explanation in terms of the interaction between the mean flow and eddy field. We use ultrasonic Doppler velocimetry to characterise the flow in a laboratory flume, reporting on the velocity field, turbulence statistics and wake structure, com-



Figure 1: This computer model of flow past Bass Point (35°S), a 4-km wide headland near Sydney, shows attached eddies and a vortex street in the headland wake (adapted from [4]).

paring cases with and without an incident disturbance. Our measurements show that wake behaviour is modified, sometimes strongly, by incident disturbances.

### Experimental Details

#### Apparatus

Experiments were conducted in a Perspex flume 3-m long, 0.4-m high and 0.75-m wide (figure 2). A semi-cylindrical vertical headland of radius  $L = 49.27 \text{ mm}$  was fixed to the side wall of the flume, extending through the depth of the flow. A cylindrical 'island' of diameter  $d = 12.6 \text{ mm}$  placed 114 mm upstream of the headland perturbs the oncoming flow.

The flume was filled with salt water to a depth  $h = 56 \text{ mm}$  or 107 mm. The flow was seeded with neutrally buoyant Griltex copolyamide particles of 60 per cent 50- $\mu\text{m}$  and 40 per cent 80- $\mu\text{m}$  diameter to reflect ultrasound for velocimetry purposes. Pumps continuously recirculated fluid through the flume.

A number of flow-calming measures were employed. At the inlet end of the flume, fluid exited pump hoses through an array of small holes in lengths of horizontal PVC pipe. The pipes extended across the full flume width. The flow then passed over a weir before entering two polycarbonate honeycombs in series—each 750-mm wide, 127-mm high and 50.8-mm long with 3.2-mm circular cells—the second of which was wrapped with wire mesh. At the outlet end of the flume, the flow again passed over a weir and through honeycomb before entering the pumps through hoses and returning to the inlet end. In between was a 2.4-m working section in which the incident disturbance and headland model were positioned.

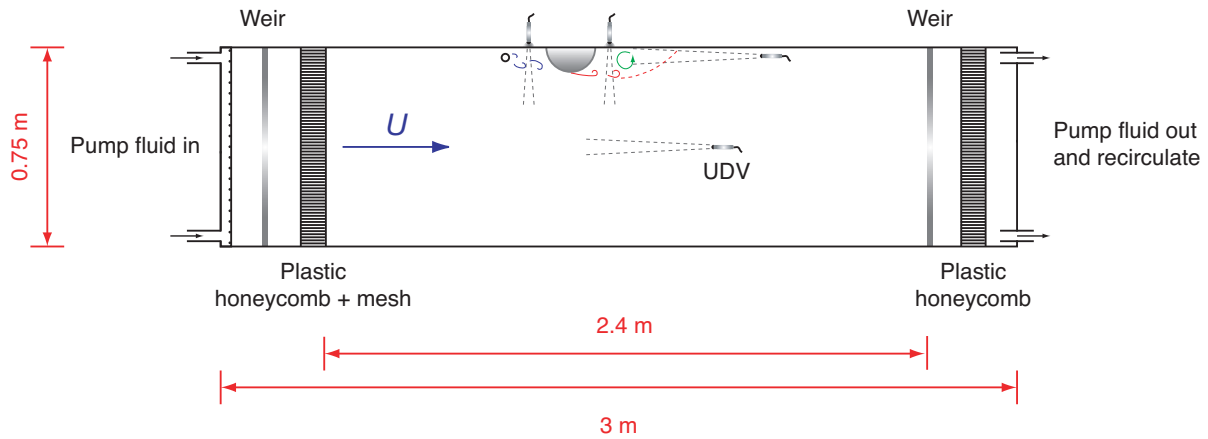


Figure 2: Plan view of experimental setup. Fluorescent tubes along the long external walls of the tank illuminate the flow; a digital video camera mounted above the flume records dye streaklines. A small acrylic cylinder upstream of the headland model generates the perturbed flow.

Pumps recirculated the flow for 10 to 15 minutes before each 20-minute experiment was started. Between each run, air bubbles and trapped particles were dislodged from the flow-straightening honeycomb and wire mesh, and the flow was thoroughly stirred.

Figure 3 defines the co-ordinate system used in this paper. We define positions downstream of the headland in terms of the dimensionless length  $x/L$  where  $x=0$  corresponds to the centre of the semi-cylindrical headland. Cross-flume positions are given as  $y/L$  where  $y=0$  corresponds to the ‘coastline’ upstream and downstream of the headland. The depth  $z=0$  at the bottom of the flume, reaching a maximum  $h$  at the free surface.

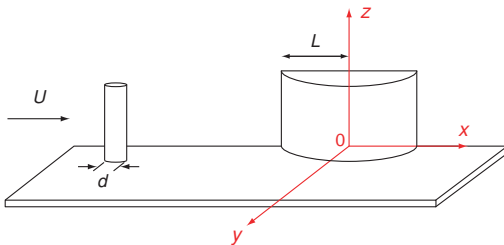


Figure 3: Schematic of obstacle geometry indicating the coordinate system, cylindrical ‘island’ perturbing the incident flow and the semi-cylindrical headland.

Our experiments were carried out with freestream  $u$ -velocities of approximately 9, 18 and  $30\text{ mm s}^{-1}$ . Taking our length scale  $L$  as the headland radius, the distance the headland intrudes into the freestream, equation (1) yields Reynolds numbers of approximately 400, 800 and 1400. We measured freestream velocity throughout each experiment, at mid-depth along the centre of the flume. We varied the Reynolds number by adjusting the number of pumps circulating the flow or by reducing the water depth  $h$  for a given flow rate.

We decompose any time-varying velocity into a mean and fluctuating component as follows:

$$u(t) = \bar{u} + u'(t), \quad (2)$$

where  $\bar{u}$  is the mean  $u$ -velocity over time and  $u'$  is the turbulent fluctuation with time.

The root-mean-square of the velocity fluctuations is thus given by

$$u_{rms} = \sqrt{u'(t)^2} = \sqrt{u(t) - \bar{u}}^2, \quad (3)$$

The freestream turbulence intensity,  $u_{rms}/\bar{u}$  at each of our flow conditions was  $\sim 3\text{--}5\%$ . This is consistent with typical open-channel turbulence intensities quoted by Chen and Jirka [3].

A digital video camera mounted 2.1-m above the flume recorded streaklines from neutrally buoyant dyes. Blue dye is released at the centreline in the lee of the upstream cylinder, red dye along the headland boundary layer upstream of the separation point, and green dye in the headland wake. Fluorescent tubes mounted on laboratory scaffolding along the external walls of the tank supplied sufficient illumination for the flow videos.

Quantitative measurements are obtained using an ultrasonic Doppler velocimeter (UDV) discussed below.

### Measurement Techniques

We use a pulsed ultrasonic Doppler velocimeter (DOP 2000, model 2125, Signal Processing S.A.) to measure the velocity field.

The UDV measuring principle is well-documented in the literature [8, 9]. Short ultrasonic pulses are emitted from a transducer through the working fluid, via a coupling medium if required. The same transducer receives the echoes which reflect from microparticles suspended in the fluid. The measured time delay from the start of a pulse burst to its reception determines the position of a sample volume of particles. At the same time, velocity information is derived from the Doppler shift frequency at that instant. We thus obtain a full profile of the along-beam component of the velocity distribution.

By definition, the velocity is positive if microparticles move away from the UDV transducer, and negative if moving towards it.

A typical transducer arrangement in this work is shown in figure 2, where the flow is from left to right. In all wake-flow experiments, one 4-MHz transducer (TR0410SS) was positioned in the centre of the flume at mid-depth, measuring the

freestream velocity over a 500-mm range. A second 4-MHz transducer placed near the coastline looked upstream towards the headland wake, allowing us to measure the length of the wake recirculation bubble. One or more 8-MHz transducers (TR0805SS) placed outside the flume, coupled with ultrasonic gel, measured the  $v$ -velocity as a function of time in the wake of the upstream cylinder or in the wake of the headland.

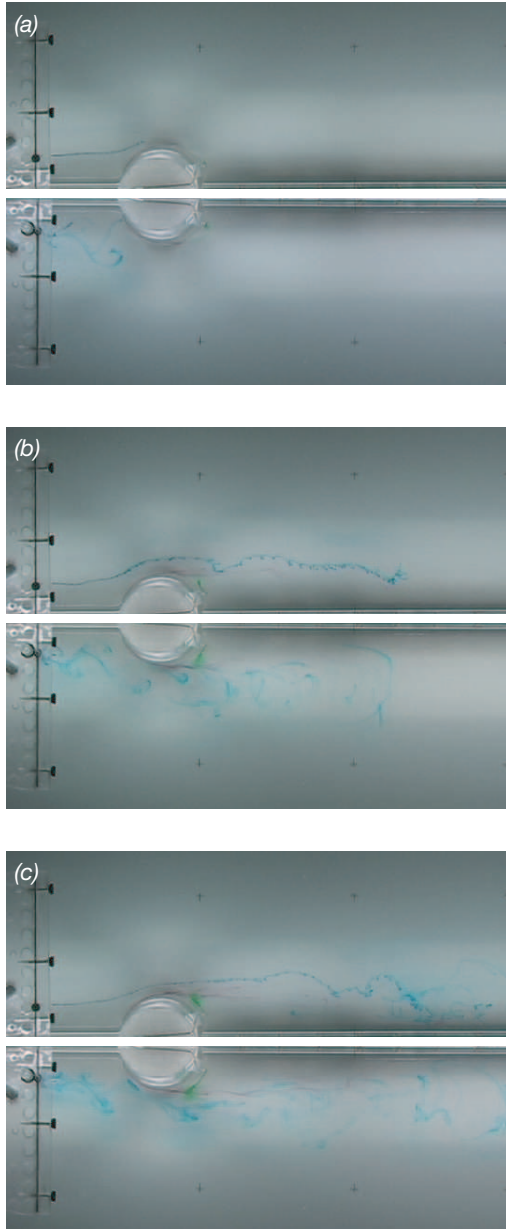


Figure 4: Still images of two experiments at a headland Reynolds number of 480. Dye streaklines indicate the influence of an incident vortex street on the headland wake (bottom image of each pair). Images in (c) were extracted 33 s after images in (b), which were obtained 33 s after (a). Flow is from left to right and the coast is a vertical wall.

#### Data Analysis

Data at each measurement gate were analysed using MATLAB. We used the algorithm of Goring and Nikora [5] to detect spikes in the record and replace spurious data with extrapolated values from the two preceding valid data points. Zero-velocity

spikes were detected on occasion, usually far along the beamline. This indicates that the measurement volume at a gate has insufficient acoustic reflection, possibly through a combination of particle settling and expansion of the beamline. The UDV manufacturer quotes a half-angle divergence of  $1.5^\circ$  for the 4-MHz transducer and  $1.2^\circ$  for the 8-MHz transducer.

## Results and Discussion

### Uniformity of the Flow Field

We denote the fluid velocity by  $\vec{u}$  with Cartesian components  $(u, v, w)$  in the  $x$ ,  $y$  and  $z$  directions, respectively, as defined in figure 3.

To assess uniformity of the flowfield, for each Reynolds number condition we measured the  $u$ -velocity at mid-depth, at points across the flume. There was less than 5% variation in streamwise velocity up to six obstacle length scales upstream of the UDV transducer, confirming fully developed oncoming flow.

Variations in  $u$ -velocity at positions across the flume were limited to 10% of the mean flow measurement within four length scales of the headland model.

### Flow Visualisation

Figure 4 shows three pairs of images at a headland Reynolds number of 480, comparing the evolution of the ‘natural’ headland wake flow with no incident disturbance (top image of each pair) and with a small cylindrical island perturbing the mean flow (bottom). Flow is from left to right, and corresponds to a regime where the freestream in the flume is unsteady.

Blue dye from upstream reveals a classic Kármán vortex street in the bottom image of each pair. This disturbance expands as dye is advected downstream. Once this perturbed flow reaches the obstacle, the vortices from upstream become more diffuse through turbulent mixing.

At this low- $Re$  condition, vortex roll-up shown by red dye in the headland wake shear does not occur in the images of natural shedding, but is induced by the oncoming perturbed flow in the bottom image of each pair.

### Velocity Profiles Across the Headland Wake

In order to build a picture of wake behaviour with and without perturbed oncoming flow, we measured  $v$ -velocities across the headland wake at eight dimensionless downstream positions  $x/L$ , for each of our three Reynolds number conditions.

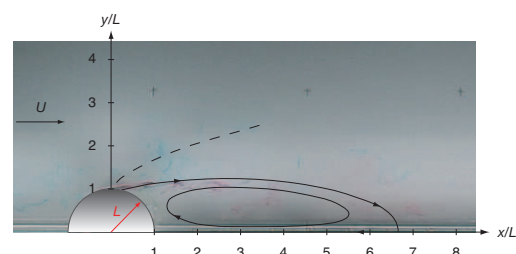


Figure 5: Schematic of mean separation streamline and wake shear layer indicating dimensionless downstream positions  $x/L$  and cross-stream positions  $y/L$ . Flow is from left to right.

An 8-MHz transducer coupled to the flume exterior using ultrasonic gel recorded the profiles, with two 4-MHz transducers present in the flow (see figure 2) to measure the mean flow speed in the centre of the flume and velocities near the wall. Due to

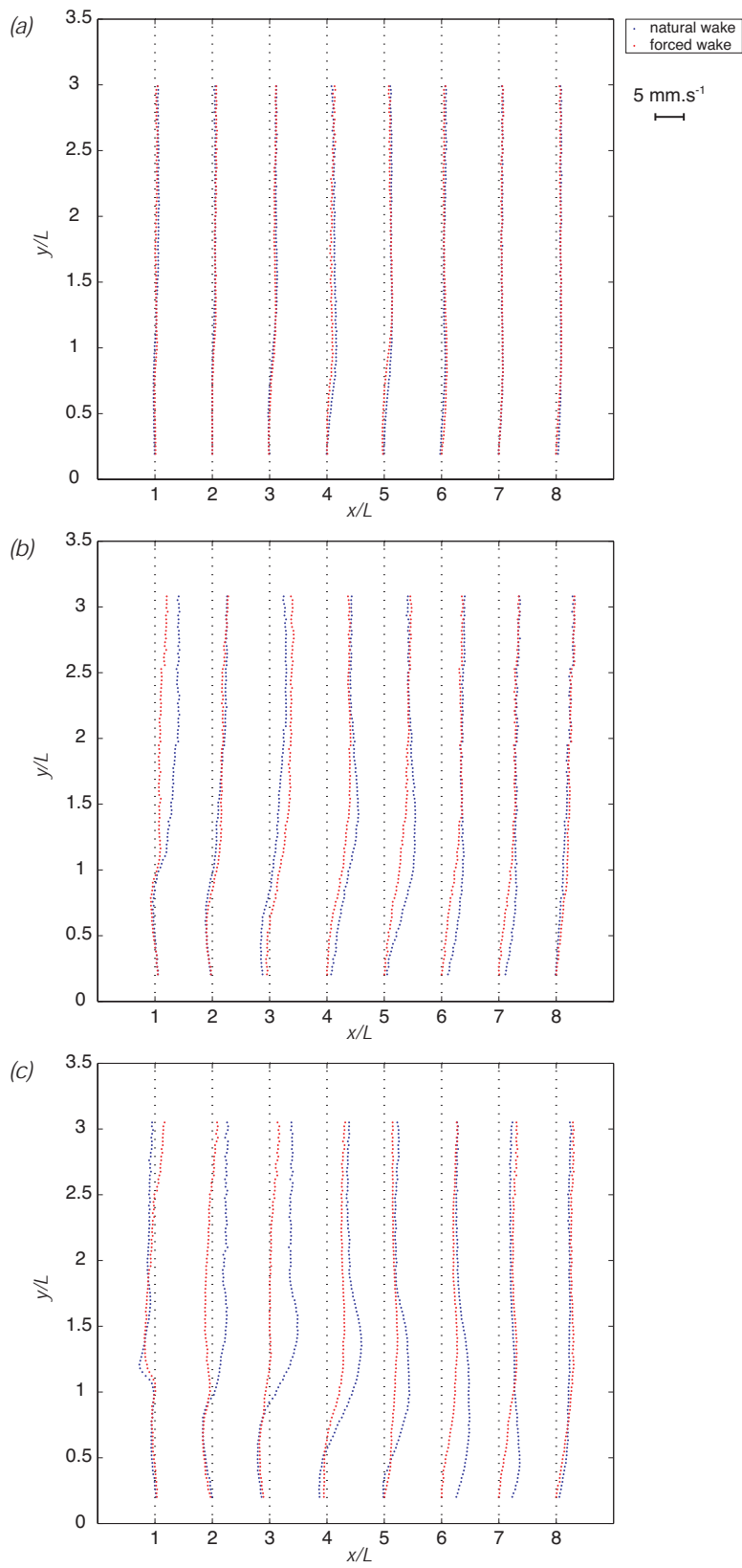
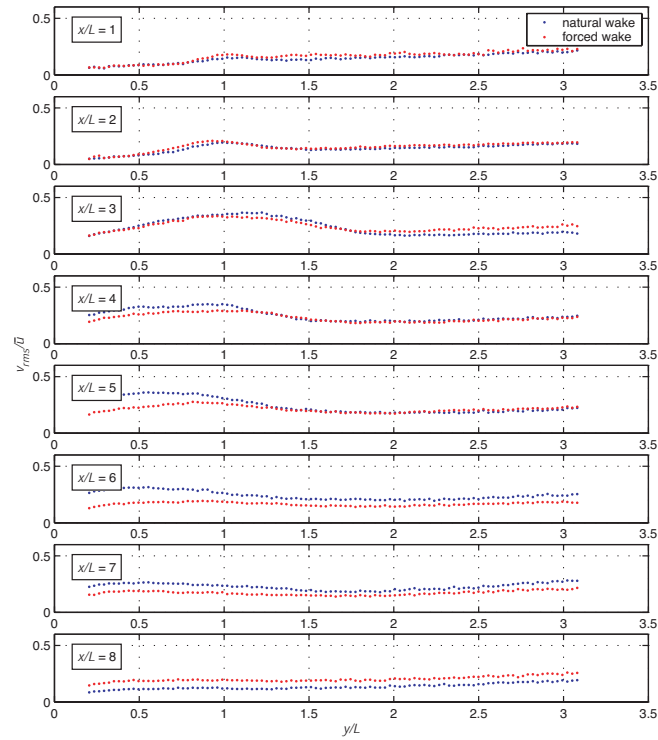


Figure 6: Mean  $v$ -velocity profiles at eight dimensionless downstream positions  $x/L$  across the headland wake, for Reynolds numbers of (a) 470, (b) 720 and (c) 1440. Grid lines represent the zero-velocity line for each profile, with positive velocities (flow moving away from the transducer) to the left of the grid lines and negative velocities (flow moving towards the transducer) to the right.

(a)



(b)

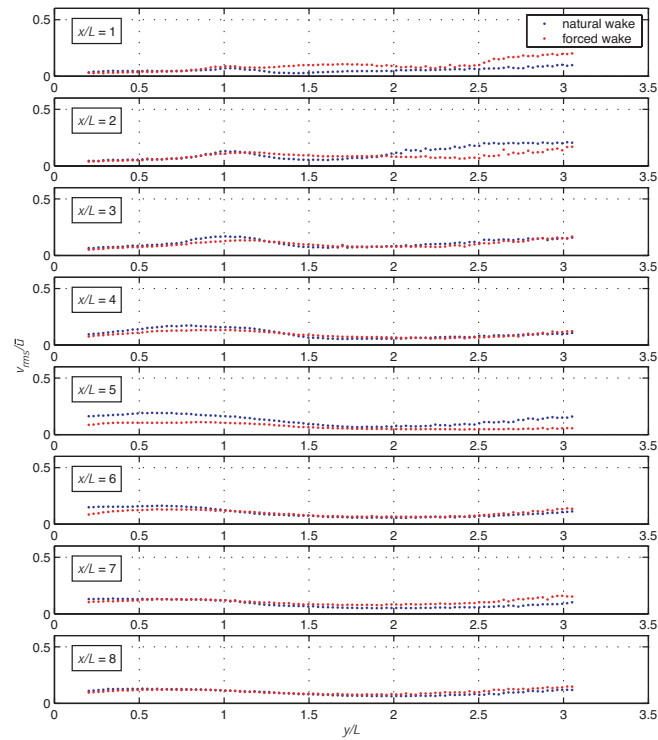


Figure 7: Root-mean-square  $v$ -velocities normalised by the mean flow velocity  $\bar{u}$ , for downstream positions  $x/L$  across the headland wake. Reynolds numbers are (a) 720 and (b) 1440.

ringing in the near field of the 8-MHz transducer, velocity profiles across the flume begin 9.5 mm in from the flume wall, and extend approximately 150 mm across the mean flow.

As shown schematically in figure 5, when a large-scale recirculating eddy is present in the lee of the headland, the mean  $v$ -velocity at downstream positions close to the obstacle is away from the wall. The transducer would thus measure a positive velocity across the wake at these positions, reaching a minimum at the outer boundary of the wake shear layer. Outside the wake, the freestream curves around the obstacle towards the wall, measured by the UDV as a negative velocity. At the furthest downstream measurement points, the mean  $v$ -velocity profiles measure only the freestream moving towards the wall.

Cross-flume velocity profiles at dimensionless downstream positions  $x/L$  are shown in figure 6 for Reynolds numbers of (a) 470, (b) 720 and (c) 1440. Each profile was calculated by averaging 2040 individual profiles at each of 100 measurement gates, with a longitudinal resolution of 1.39 mm.

Grid lines show the zero-velocity line for each pair of profiles, for the case of a natural headland wake and for the forced wake with upstream perturbation. To the left of this line, fluid moves away from the transducer, corresponding to a positive velocity. Data points to the right of this line show motion towards the UDV transducer, or a negative velocity. A  $5 \text{ mm s}^{-1}$  bar indicates the scale of the velocity fluctuations in the  $y$  direction.

It is clear that at the low Reynolds number condition, the presence of an incident disturbance has little effect on the flow. At the mid-range condition of  $Re = 720$ , the effect is more pronounced, and at the faster condition corresponding to a  $Re = 1440$ , the incident disturbance has a dramatic effect on the flow.

We note with interest that the first pair of profiles at the high Reynolds number condition (figure 6(c)), taken across the flow directly behind the obstacle at  $x/L = 1$ , indicate a slightly positive velocity near  $y/L = 1$ . This means that the oncoming flow, whether perturbed or not, has plucked the separated flow away from the obstacle towards the centre of the flume.

These across-wake velocity profiles, particularly (b) and (c), also tell us something about the energetics of the flowfield. Beginning at  $x/L = 1$  in (b), we see that the mean speed across the wake is slightly greater in the case of forced or perturbed flow, shown in red, but further into the flow for  $y/L \geq 1$  the speed of the forced flow is less than that for the natural flow. This trend continues as we move downstream of the headland to greater  $x/L$ : the mean velocity in all cases with an incident disturbance decays far more rapidly than the mean velocity with no disturbance.

The perturbed wakes show a lot less across-stream variation than the natural wakes. We speculate that this may be due to a larger effective horizontal diffusion associated with the incident disturbance.

### Turbulent Velocity Fluctuations

As defined in equation 3, we subtract the time-varying velocity component in the  $y$ -direction,  $v(t)$ , at each measurement gate from the mean  $v$ -velocity profiles to calculate the root-mean-square (RMS) of the velocity fluctuations across the flow,  $v_{rms}$ .

Root-mean-square  $v$ -velocities normalised by the mean flow speed in the  $x$ -direction,  $\bar{u}$ , are plotted in figure 7 for the two higher Reynolds numbers of interest. We omit the low- $Re$  case here as variability with downstream position or with a disturbance was minimal, as is clear from figure 6(a).

In the case of perturbed flow, RMS  $v$ -velocities near the headland strongly fluctuate, intruding at least three length scales into the flow. Blue dye released from the small upstream cylinder in the lower sets of images in figure 4 further support this.

Note that velocity fluctuations are greatest in the shear layers, which is consistent with a larger effective diffusion of momentum through these regions.

### Effects of Incident Disturbances on Shear-Layer Width

Middleton *et al.* [7] report that topographically generated turbulence appears to prevent the formation of a narrow shear layer, and instead provides a much wider shear layer where the non-linear terms are less effective at rolling up the flow to form a large-scale recirculation.

If we take maxima in each dimensionless RMS profile to be the centre of the shear layer, with minima either side of that representing the extent of that shear layer, we can use the profiles in figure 7 to study the width of the shear layers in our experiments. Using this thresholding condition, we estimate the shear-layer width to be the length scale between those dimensionless RMS velocities 10% greater than the measured minima.

These measurements are plotted in figure 8 for the two highest Reynolds number conditions of 720 and 1440, respectively. At  $Re = 1440$  there is a pronounced difference in structure of the perturbed wake (in red) to the natural one (in blue). The open circles and dashed lines signify that the outer boundary of the shear layer is likely to be directly affected by the vortex street coming from upstream. Dye streaklines show that, in reality, the shear-layer width close to the headland is considerably greater than indicated in this figure.

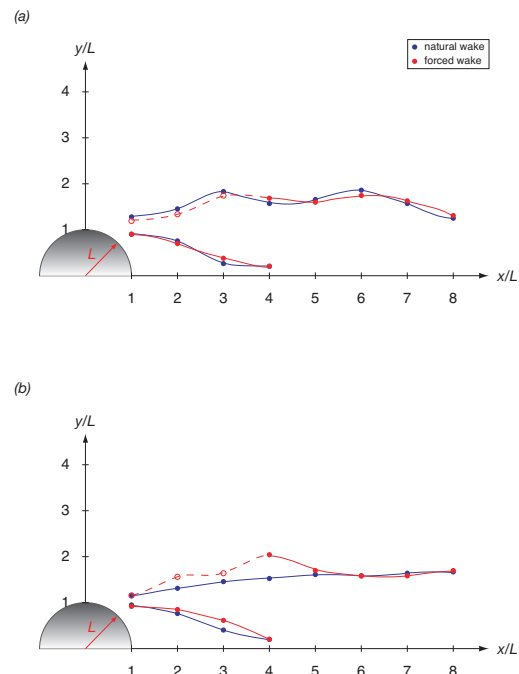


Figure 8: Smoothed lines indicate the inferred boundary of the shear layer at (a)  $Re = 720$  and (b)  $Re = 1440$  with and without perturbed incident flow.

Due to near-field effects with the transducer, there is a region close to the coastline where velocities are not measurable. For this reason, the lower bound of the shear layers in figure 8 look to stop at  $x/L = 4$  regardless of Reynolds number. This is simply

a measurement limitation, not an indication of the length of the headland wake.

### Effects of Incident Disturbances on Wake Length

We have discussed two UDV transducers thus far, one that measures the mean  $u$ -velocity in the centre of the flume and one that measures the fluctuating  $v$ -velocity across the headland wake at different downstream positions.

A third transducer in each experiment enables us to measure the distance from the headland to the wake stagnation point. This transducer is 20 mm in from the coastline, looking upstream towards the obstacle which is 484-mm away, as shown schematically in figure 2.

Within the wake, microparticles move away from the transducer, and the measured velocity is therefore positive in sign. Fluid outside the wake, whether in the shear layer or freestream, moves towards the transducer. Therefore we identify the end of the wake by the point where the mean velocity profile from this transducer crosses zero.

Dimensionless wake length as a function of  $Re$  is plotted in figure 9 for the natural and perturbed wake cases. Each data point represents the mean wake length calculated from 1020 profiles. Error bars give the standard error in the mean.

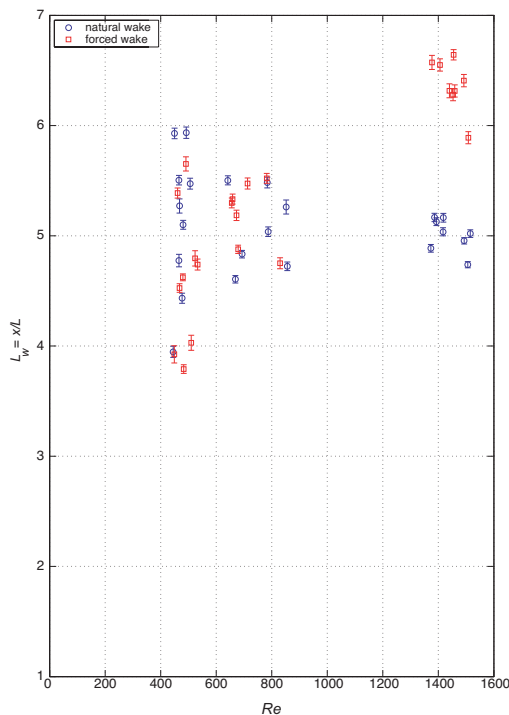


Figure 9: Wake length  $L_w$  for natural (circles) and forced (squares) wakes, expressed as  $x/L$ , as a function of Reynolds number.

We find that for low  $Re$ , the forced wake is almost always shorter than the natural wake, by a fraction of a length scale. At higher Reynolds numbers of around 800, there seems to be a transition where the forced wake is usually longer than the natural case, but not exclusively so. And in experiments to date, at  $Re = 1400$  the forced wake is always at least one length scale greater than the natural wake.

Figures 6, 8 and 9 form a complete picture of the headland wake and shear layer with and without incident disturbances.

### Conclusions

We have studied the effects of an incident flow disturbance on the wake structure and behaviour of a simple headland model at three Reynolds number conditions of relevance to coastal oceans. We have measured mean velocity profiles across the wake, turbulent  $v$ -velocity fluctuations and we have measured the length of each headland wake. We find that velocity fluctuations are greatest in the shear layers, and this is especially evident at higher Reynolds numbers. Across the flow, we see a smearing in the dimensionless  $v_{rms}$  velocities, with minimal variation across-stream but of a consistently high magnitude. We speculate that this is due to a larger effective horizontal diffusion associated with the incident disturbance. In the coastal oceans, this may translate as nutrients, sediments or pollutants being swept off the continental shelf far more rapidly when an upstream influence perturbs the oncoming flow.

### Acknowledgements

The authors gratefully acknowledge the support of the Australian Research Council. We thank Tony Beasley and Daniel Hunt for their technical assistance in constructing and modifying the laboratory flume.

### References

- [1] Aiken, C. M., Moore, A. M. and Middleton, J. H., The non-normality of coastal ocean flows around obstacles, and their response to stochastic forcing, *J Phys Oceanogr*, **32**, 2002, 2955–2974.
- [2] Batchelor, G., *An Introduction to Fluid Dynamics*, Cambridge University Press, 1970.
- [3] Chen, D. and Jirka, G. H., Experimental study of plane turbulent wakes in a shallow water layer, *Fluid Dyn Res*, **16**, 1995, 11–41.
- [4] Denniss, T., Middleton, J. H. and Manasseh, R., Recirculation in the lee of complicated headlands: A case study of Bass Point, *J Geophys Res-Oceans*, **100**, 1995, 16087–16101.
- [5] Goring, D. G. and Nikora, V. I., Despiking acoustic Doppler velocimeter data, *J Hydraul Eng*, **128**, 2002, 117–126.
- [6] Middleton, J., Topographic eddies, in *Encyclopedia of Ocean Sciences*, Academic Press, 2001, volume 6, 2986–2993.
- [7] Middleton, J. H., Griffin, D. A. and Moore, A. M., Oceanic circulation and turbulence in the coastal zone, *Cont Shelf Res*, **13**, 1993, 143–168.
- [8] Takeda, Y., Velocity profile measurement by ultrasonic Doppler method, *Exp Therm Fluid Sci*, **10**, 1995, 444–453.
- [9] Willemetz, J.-C., *Etude quantitative de l'hémodynamique de vaisseaux profonds par échographie Doppler ultrasonore*, Ph.D. thesis, Ecole Polytechnique Fédérale de Lausanne, Switzerland, 1990, Thèse no. 893.